

## Reversing Electron Transfer in Covalent Triazine Framework for Efficient Photocatalytic Hydrogen Evolution

Linwen Zhang,<sup>a,c</sup> Yaoming Zhang,<sup>b</sup> Xiaojuan Huang,<sup>a</sup> Yingpu Bi<sup>a,d\*</sup>

<sup>a</sup> State Key Laboratory for Oxo Synthesis & Selective Oxidation, National Engineering Research Center for Fine Petrochemical Intermediates, Lanzhou Institute of Chemical Physics, CAS, Lanzhou, Gansu 730000, P. R. China.

<sup>b</sup> Key Laboratory of Science and Technology on Wear and protection of Materials, Lanzhou Institute of Chemical Physics, CAS, Lanzhou 730000, P. R. China.

<sup>c</sup> Qingdao Key Laboratory of Functional Membrane Material and Membrane Technology, Qingdao Institute of Bioenergy and Bioprocess Technology, CAS, Qingdao 266101, China.

<sup>d</sup> Dalian National Laboratory for Clean Energy, CAS, Dalian 116023, China.

\*Corresponding author, E-mail: [yingpubi@licp.cas.cn](mailto:yingpubi@licp.cas.cn)

## Experiment section

### Chemicals and reagents

1,4-Benzenedimethanol, terephthalamidine dihydrochloride and cesium carbonate ( $\text{Cs}_2\text{CO}_3$ ) were of analytical grade and purchased from National Medicines Corporation Ltd. of China. Cobaltous nitrate hexahydrate, Sodium hypophosphite, ammonium hydroxide, hydrochloric acid and tetrahydrofuran were obtained from Sinopharm Chemical Reagent Co., Ltd. Deionized water with a resistivity of  $18.25 \text{ M}\Omega \cdot \text{cm}^{-1}$  was used in all reactions.

### Characterizations

Transmission electron microscopy (TEM) measurements were performed by using a FEI Tecnai TF20 microscope operated at 200 kV. The crystalline structures were identified by X-ray diffraction analysis (XRD, Smartlab-SE) using  $\text{Cu K}\alpha$  radiation at 50 kV and 50 mA. The elemental composition and chemical valence state were determined by X-ray photoelectron spectroscopy (XPS, ESCALAB 250Xi). A 300 W Xe arc lamp was used as illumination source in SI-XPS tests. UV-visible diffuse reflectance spectra were performed on a UV-2550 (Shimadzu) spectrometer by using  $\text{BaSO}_4$  as the reference. Photoluminescence spectra (PL) were obtained by Edinburgh LP 980 spectrophotometer with a 355nm pulse laser as the excitation source and a xenon lamp as probe light. Fourier transform infrared spectroscopy (FTIR) results of samples were recorded on a Thermo Nicolet NEXUS TM spectrophotometer. The loadings of  $\text{Co}_2\text{P}$  were measured on inductively coupled plasma-atomic emission spectrometer (ICP-AES) on a VistaChip II CCD detector (Agilent 725-ES). Brunauer-Emmet-Teller (BET) specific surface area of the as-prepared materials was measured via automatic specific surface area measuring equipment (ASAP 2020M, USA). Solid-state nuclear magnetic resonance (NMR) experiments were carried out on a Varian Infinityplus-300 spectrometer with a 4 mm double-resonance MAS probe. NEXAFS Measurements: The O K-edge X-ray absorption fine structure spectroscopy (XAFS) was measured at the U7C station of National Synchrotron Radiation Laboratory (NSRL) China. The storage ring of the NSRL was operated at 0.8 GeV with a maximum current of 200 mA.

### Preparation of covalent triazine-based frameworks (CTF)

The method was reported by the Tan's group in 2018.<sup>[1,2]</sup> 1,4-Benzenedimethanol (69 mg, 0.5 mmol), terephthalamidine dihydrochloride (235 mg, 1.0 mmol), and cesium carbonate (716 mg, 2.2 mmol) were added to the dimethyl sulfoxide solution (15.0 mL) in a round-bottom flask (25 mL). The mixture was heated at 100 °C for 10 h and then up to 180 °C for 36 h. The precipitates of the yellow suspension were washed with dilute hydrochloric acid

(1M,  $3 \times 10$  mL) to remove residual cesium carbonate, and further washed with water ( $3 \times 10$  mL), ethanol ( $3 \times 10$  mL), and tetrahydrofuran ( $3 \times 10$  mL). The filtered solids were dried in vacuum oven for 24 h to yield CTF as a yellow power (150 mg, 84% yield).

### **Preparation of P-CTF-Co<sub>2</sub>P**

The 0.5, 1, 2 or 4 mg Co(NO<sub>3</sub>)<sub>2</sub> and 10 mg CTF were mixed with 60 mL water, then treating with sonication for 1 h to form a homogeneous dispersion. Afterward, 1 mL NH<sub>3</sub>·H<sub>2</sub>O was added into dispersion solution and stirred for 30 mins. Then, the mixtures were washed with distilled water and ethanol several times, and then dried in an oven at 60 °C, denoted as CTF-Co(OH)<sub>2</sub>. Then, the samples were grinded with NaH<sub>2</sub>PO<sub>2</sub>·H<sub>2</sub>O with mass ratio at 1:5, then the solid powder was heated in argon atmosphere at 250°C for 90 mins with a ramp of 4°C/min and cooled naturally to room temperature. At last, the obtained samples were washed with distilled water and ethanol several times, and then dried in an oven at 60 °C to obtain the catalyst. The resulting catalysts were denoted as P-CTF-Co<sub>2</sub>P-1, P-CTF-Co<sub>2</sub>P, and P-CTF-Co<sub>2</sub>P-2. The optimum photocatalytic hydrogen evolution is simplified as P-CTF-Co<sub>2</sub>P. The detailed contents of Co<sub>2</sub>P in catalysts were measured by the inductively coupled plasma-atomic emission spectrometer (ICP-AES). The average Co<sub>2</sub>P loading values of all catalysts are calculated to be 1wt%, 2wt% and 4wt% from ICP results, respectively.

### **Preparation of P-CTF**

The 100 mg CTF were grinded with NaH<sub>2</sub>PO<sub>2</sub>·H<sub>2</sub>O (100 mg) and then heated in argon atmosphere at 250°C for 90 mins with a ramp of 4°C/min. At last, the obtained samples were washed with distilled water and ethanol several times, and then dried in an oven at 60 °C to obtain the catalyst.

### **Preparation of CTF/Co<sub>2</sub>P and P-CTF/Co<sub>2</sub>P**

The catalyst was first prepared by adding CTF (100 mg) into 60 mL of deionized water and then treating with ultrasonication to form a homogeneous dispersion. Afterward, the 2 mg Co<sub>2</sub>P were added into CTF dispersion with sonication for 2h and stirred overnight. Then, the mixture was dried in an oven at 60 °C, and heated in argon atmosphere at 250°C for 90 mins with a ramp of 4°C/min and cooled naturally to room temperature, resulting in CTF/Co<sub>2</sub>P. The photocatalyst of P-CTF/Co<sub>2</sub>P was prepared following the same processes by replacing CTF by P-CTF.

### **Preparation of P-CTF-Co<sub>2</sub>P-Co**

The 10 mg P-CTF-Co<sub>2</sub>P were added into 60 mL water, and then treated with sonication for 30 min to form a homogeneous dispersion. Afterwards, 10 mg Co(NO<sub>3</sub>)<sub>2</sub>·6H<sub>2</sub>O was added into the mixed solution and stirred with for 1 h. Then, the sample was collected by centrifugation to obtain P-CTF-Co<sub>2</sub>P-Co catalysts.

### **Preparation of P-CTF-Co<sub>2</sub>P-Pt**

The 10 mg P-CTF-Co<sub>2</sub>P were added into 60 mL water, and then treated with sonication for 30 min to form a homogeneous dispersion. Afterwards, Pt cocatalysts were deposited by in-situ photo-deposition strategy from H<sub>2</sub>PtCl<sub>6</sub> precursor (80 μL, 19.3 mmol L<sup>-1</sup>) under 30 min. Then, the sample was collected by centrifugation to obtain P-CTF-Co<sub>2</sub>P-Pt catalysts.

### **Preparation of CTF-Pt samples**

The 50 mg CTF was added into 100 mL of aqueous solution (0.1 M NaOH, 0.1 M NaBH<sub>4</sub>), treating with ultrasonication to form a homogeneous dispersion. The desired amount of H<sub>2</sub>PtCl<sub>6</sub> aqueous solution (0.13, 0.26, 0.39, 0.52 or 0.65 mL, 19.3 mmol·L<sup>-1</sup>) was added into dispersion solution. Subsequently, the solution was stirred for 120 mins and washed with water and ethanol. Finally, the as-obtained sample was dried in oven at 60°C.

### **Photocatalytic H<sub>2</sub> evolution activity measurements**

The photocatalytic reactions were carried out in a Pyrex top-irradiation reaction vessel connected to a closed gas circulation and evacuation system. H<sub>2</sub> production was performed by dispersing 10 mg of catalyst powder in an aqueous solution (50 mL) containing triethanolamine (10 vol%) as a sacrificial electron donor. The photocatalysis experiments was performed under the vacuum state, in which the pressure was about 0.7~0.9 KPa. The reactant solution was degassed several times to remove air prior to irradiation under a 300 W Xenon lamp (PLS-SXE300, PerfectLight Technology Co, Ltd., Beijing). The temperature of the reaction solution was maintained at 8°C by the flow of cooling water during the reaction. The amount of H<sub>2</sub> production was analyzed using an online gas chromatography (Agilent Technologies, 7890A).

AQY measurement: The apparent quantum yield (AQY) for H<sub>2</sub> evolution was measured under the same reaction conditions using different band-pass filter. Depending on the amounts of hydrogen gases produced by the photocatalytic reaction in an average of one hour, the AQY was calculated as follow:

$$\eta_{AQY} = \frac{2 \times \text{the number of evolved hydrogen molecules}}{\text{the number of incident photos}} \times 100\%$$

$$\begin{aligned}
& \frac{N_e}{N_p} \times 100\% = \frac{2 \times M \times N_A}{E_{\text{total}} E_{\text{photon}}} \times 100\% \\
& \frac{2 \times M \times N_A}{S \times P \times t} \\
& = \frac{h \times \frac{c}{\lambda}}{S \times P \times t \times \lambda} \times 100\% = \frac{2 \times M \times N_A \times h \times c}{S \times P \times t \times \lambda} \times 100\%
\end{aligned}$$

where M is the amount of H<sub>2</sub> molecules (mol), N<sub>A</sub> is Avogadro constant (6.022 × 10<sup>23</sup>/mol), h is the Planck constant (6.626 × 10<sup>-34</sup> JS), c is the speed of light (3 × 10<sup>8</sup> m/s), S is the irradiation area (15.2 cm<sup>2</sup>), P is the intensity of irradiation light (W/cm<sup>2</sup>), t is the photoreaction time (s), and λ is the wavelength of the monochromatic light (m), the AQY were calculated as 31.8% and 11.2 % at 365 and 405 nm, respectively.

### Photoelectrochemical measurements

All photoelectrochemical measurements were carried out on an electrochemical workstation (CHI 760D) in a three-electrode system and 0.2 mol·L<sup>-1</sup> Na<sub>2</sub>SO<sub>4</sub> (pH = 6.8) solution as electrolyte solution under 300W xenon lamp light. The sample photoelectrode, a saturated calomel electrode (SCE) and a Pt wire were served as the working electrode, reference electrode and counter electrode, respectively. In addition, the working electrodes were prepared by drop-coating sample suspensions directly onto the precleaned Fluorine-doped Tin Oxide glass (FTO glass) surface. In detail, the catalysts powder (2 mg) was dispersed into 2 mL deionized water containing 20 ul Nafion under ultrasonic treatment for 60 min to prepare the uniform dispersion. The 50 μL mixture solution was drop-coated onto the FTO glass and was dried in oven at 60°C.

### In-situ Fourier transform infrared measurements

The synchronous illumination diffuse reflectance Fourier transform infrared spectroscopy (SI-DRIFTS) was performed on Bruker VERTEX 70 infrared spectrometer equipped with the Harrick reaction cell (Model HVC-DRP-5) with ZnSe and quartz windows. The quartz window was utilized for the transmission of the UV-vis light provided by a xenon lamp (PLS-SXE300, PerfectLight Technology Co, Ltd., Beijing). After the samples were purged by Ar and H<sub>2</sub>O steam for 30 min to reaching the adsorption equilibrium, the background spectrum in the presence of the sample was collected. Next, FTIR spectra were recorded as a function of time to investigate the dynamics of the reactant desorption/conversion under visible irradiation.

### Synchronous illumination X-ray photoelectron spectroscopy (SI-XPS)

Differently from the normal XPS instrument (ESCALAB 250Xi), a 300 W Xe arc lamp was used as illumination source in SI-XPS tests for providing the simulated solar-light with full spectrum. In the process of measurements, the changes of XPS spectra were recorded by controlling light on or off at given time intervals. The samples were firstly dipped in water solution for 12 h to achieve the adsorption equilibrium, and then dried by nitrogen purging for removing the non-absorbed water. Subsequently, the obtained samples were put in pretreatment chamber of XPS equipment for 12 h to remove the physically absorbed water molecules. Finally, the samples were transferred to the analysis chamber to perform the SI-XPS measurements.

## Additional Figures and Discussions

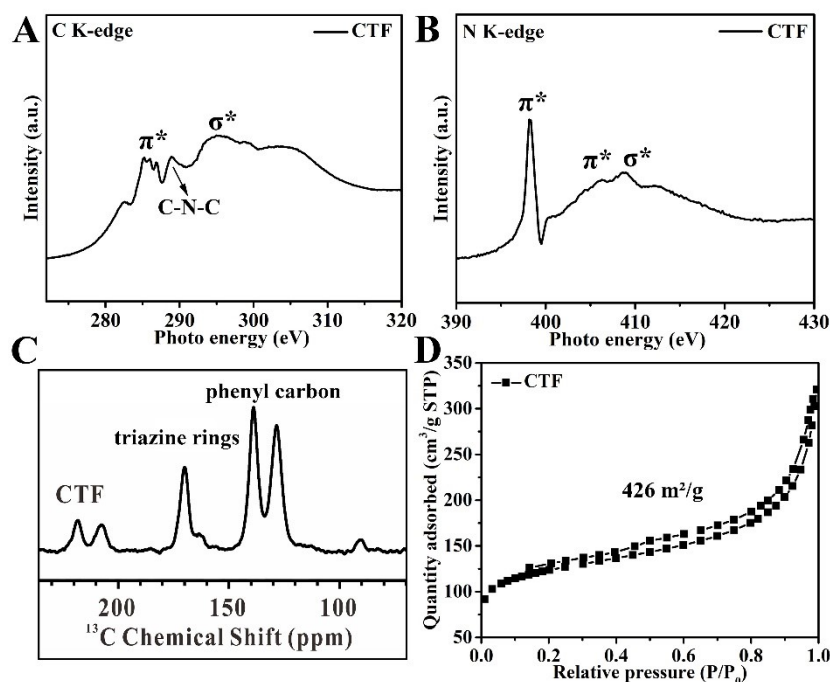


**Figure S1.** (A) C K-edge, (B) N K-edge XANES spectra, (C) solid-state  $^{13}\text{C}$  NMR spectra and (D) Nitrogen sorption curves of CTFs.

### Additional discussion:

Firstly, X-ray absorption near edge structure (XANES) spectra has been conducted to explore the coordination environment of C and N atoms in CTFs. As shown in C K-edge XANES spectra (Figure S1A), the peaks in the range of 285-287 eV could be assigned to  $\pi^*$  resonance, the peak located at  $\sim 288.9$  eV should be attributed to C-N-C coordination, and the broad peak at  $\sim 294.8$  eV could be indexed to the  $\sigma^*$  resonance.<sup>3-5</sup> The N-edge XANES spectra of the obtained CTF samples are shown in Figure S1B. More specifically, the sharp peak (398.2 eV) and broad peak (408.6 eV) could be assigned to  $\pi^*$  excitations of the pyridinic (C-N-C) and graphitic (N-3C) N species, while the broad peak centered at  $\sim 410$  eV could be indexed to  $\sigma^*$  resonance owing to the superposition of graphite-like and pyridine-like nitrogen.<sup>6,7</sup>

Furthermore, the  $^{13}\text{C}$  solid-state NMR shown in Figure S1C clearly demonstrated three obvious signals, in which the chemical shifts at 128.0 and 139.0 ppm could be assigned to phenyl

carbons and the chemical shift at 170.0 ppm should be attributed to the carbon signal from triazine rings.<sup>8-10</sup> Additionally, their surface areas and pore dimensions have also been evaluated based on Brunauer-Emmett-Teller (BET) and Langmuir methods, respectively. As shown in Figure S1D, except for the micropores resulting from the aggregated particles, the macropores and mesopores have been clearly detected in these CTF samples. The calculated surface area is 426 m<sup>2</sup>/g, which is similar to that of the reported CTF samples.<sup>11-13</sup>

On the basis of above results, the CTFs utilized in this work was generally consistent with that of the previous reports.

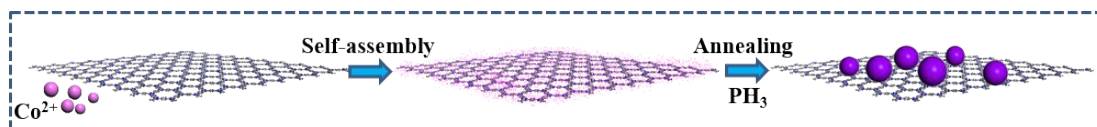


**Figure S2.** The basic procedures and the ideal structure for fabricating the metal-free P-CTF-Co<sub>2</sub>P photocatalysts.

#### **Additional discussion:**

Figure S2 shows the basic procedures for fabricating P-CTF-Co<sub>2</sub>P photocatalysts. The polymeric CTF semiconductors were fabricated by reported method, and Co<sup>2+</sup> ions were firstly adhered on the surface of CTF by the electrostatic interaction. After heating in Ar atmosphere, PH<sub>3</sub> released from the thermal decomposition of NaH<sub>2</sub>PO<sub>2</sub>, resulting in the phosphatization reaction to form the final Co<sub>2</sub>P cocatalysts and implant P element into crystals. Apart from the in-situ reduction, NaH<sub>2</sub>PO<sub>2</sub> is also responsible for the doping in precursor as P source. Finally, the P-CTF-Co<sub>2</sub>P photocatalysts were obtained.

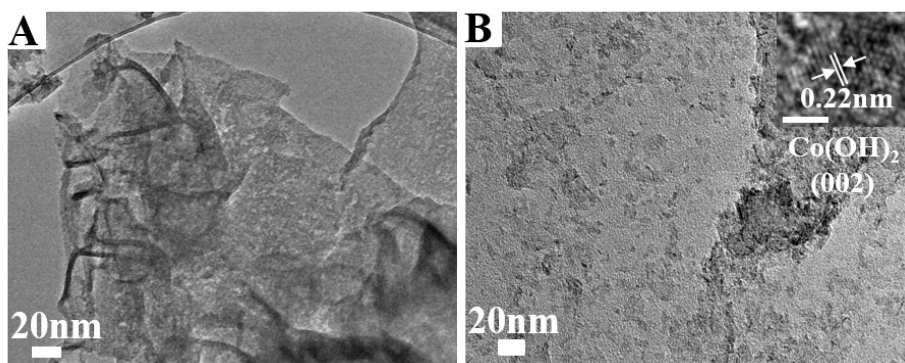


**Figure S3.** TEM images of pure CTF (A) and CTF-Co(OH)<sub>2</sub> (B) samples.

**Additional discussion:**

As shown in Figure S3, The product of intermediate step was CTF-Co(OH)<sub>2</sub> in which the Co(OH)<sub>2</sub> uniformly grown on the surface of CTF. The distinct lattice fringes with the d spacing of 0.22 nm assigned to Co(OH)<sub>2</sub> (002) planes can be observed in the high-resolution TEM (HR-TEM) image.<sup>14</sup>

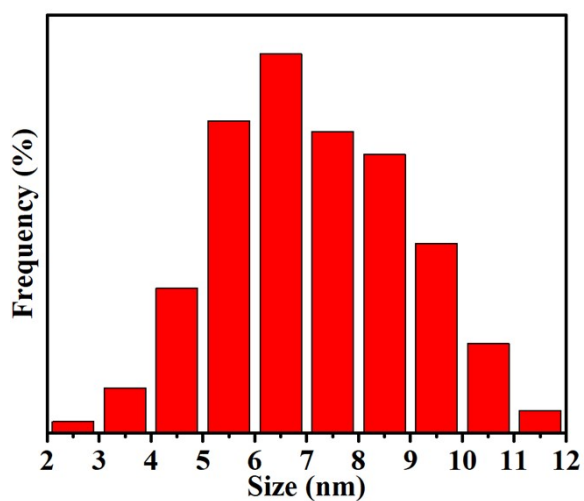


**Figure S4.** Size distribution of Co<sub>2</sub>P nanoparticles in P-CTF-Co<sub>2</sub>P.

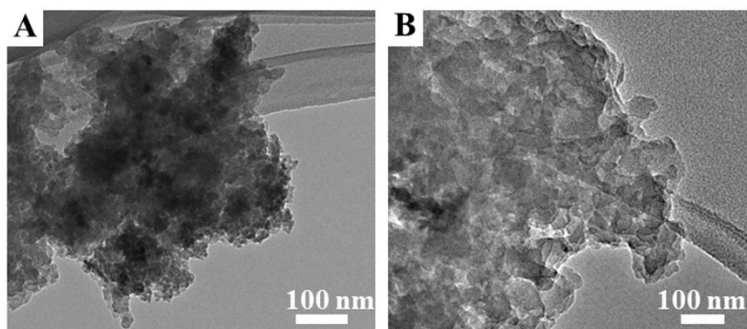


**Figure S5.** TEM image of CTF/Co<sub>2</sub>P sample before (A) and after (B) photocatalytic experiment.

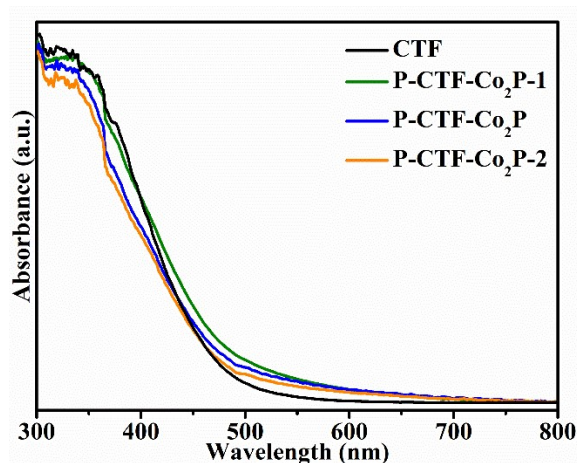


**Figure S6.** The UV-VIS spectroscopy of pure CTF and P-CTF-Co<sub>2</sub>P samples.

#### **Additional discussions:**

Their optical properties have been explored by UV-vis diffuse reflection spectra. As shown in Figure S6, compared with pure CTF, the absorption intensity of P-CTF-Co<sub>2</sub>P catalyst has been slightly enhanced, which should be ascribed to the low content of Co<sub>2</sub>P. This phenomenon demonstrated that the spectral absorption was not the decisive factor for effectively hydrogen evolution.

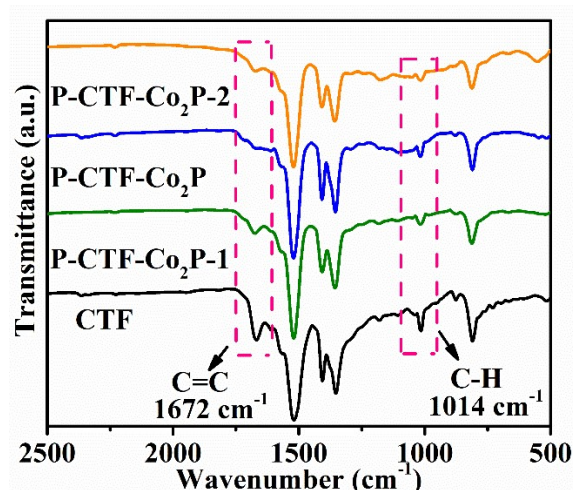


**Figure S7.** the Fourier transform infrared spectroscopy (FT-IR) of P-CTF-Co<sub>2</sub>P samples.

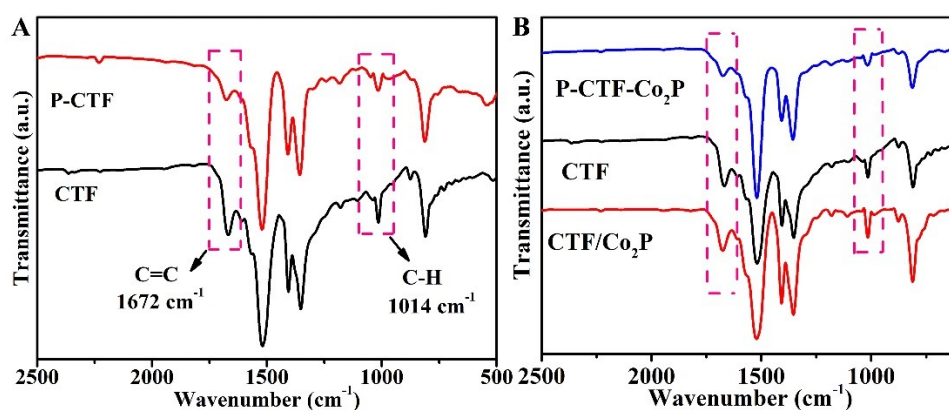


**Figure S8.** the Fourier transform infrared spectroscopy (FT-IR) of CTF, P-CTF and CTF/Co<sub>2</sub>P samples.

### **Additional discussion:**

From the result of FTIR, it can be clearly observed that P-CTF-Co<sub>2</sub>P, P-CTF and CTF/Co<sub>2</sub>P samples exhibited the similar peaks with pristine CTF. However, note that compared with pristine CTF, the peaks of 1672 cm<sup>-1</sup> and 1014 cm<sup>-1</sup> corresponding to stretching vibrations of C=C and C-H have been decreased in P-CTF-Co<sub>2</sub>P and P-CTF samples, which means that the P atoms bonding with C atoms in the benzene rings attributed to the reduced amount of benzene rings. Otherwise, there is no obvious peaks changes between CTF/Co<sub>2</sub>P and CTF samples which means that the bonding of P atoms will not occur in CTF/Co<sub>2</sub>P complex without one-pot phosphidation process.

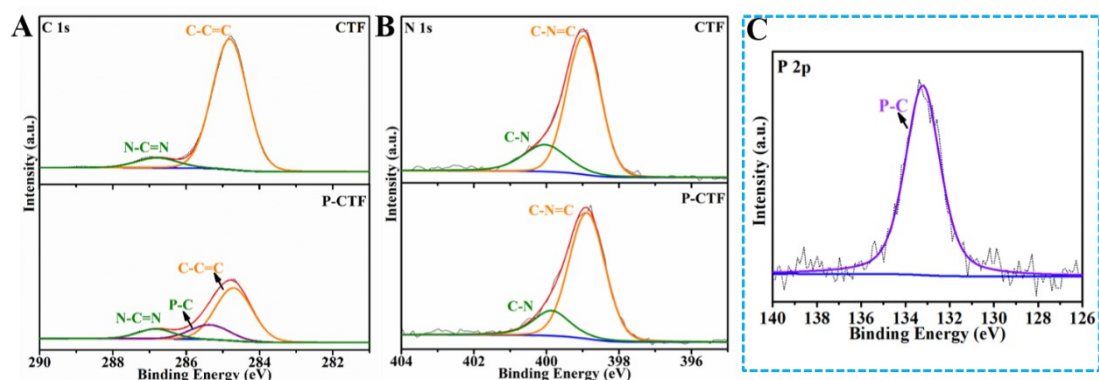


**Figure S9.** High-resolution (A) C 1s, (B) N 1s and (C) P 2p XPS spectra of P-CTF sample.

**Table S1.** The relative ratio of C-C=C to N-C=N bonds of CTF, P-CTF and P-CTF-Co<sub>2</sub>P samples.

Photocatalyst	The peak area of C-C=C (S <sub>1</sub> )	The peak area of N-C=N (S <sub>2</sub> )	The relative ratio of S <sub>1</sub> /S <sub>2</sub>
CTF	71681.4	7025.8	10.2
P-CTF	9945.6	1800.2	5.5
P-CTF-Co <sub>2</sub> P	24901.0	3511.5	7.1

#### Additional discussion:

As shown in Figure S9, the emergence of new peak at the 285.3 eV in C 1s spectrum and the P-C peak at 133.2 eV in P 2p spectrum have been observed in the P-CTF samples, similar to P-CTF-Co<sub>2</sub>P, demonstrating P atoms bonding with C atoms of benzene rings in CTFs after phosphidation treatment. The ratios of C-C=C to N-C=N bonds have been evidently decreased from 10.2 to 5.5 (Table S1), clearly revealing the evidently reduced amount of benzene rings bonded by P atoms. The reason for the different ratios of P-CTF and P-CTF-Co<sub>2</sub>P was that the partial P atoms were involved in phosphatization reaction and transformed into Co<sub>2</sub>P in P-CTF-Co<sub>2</sub>P sample.

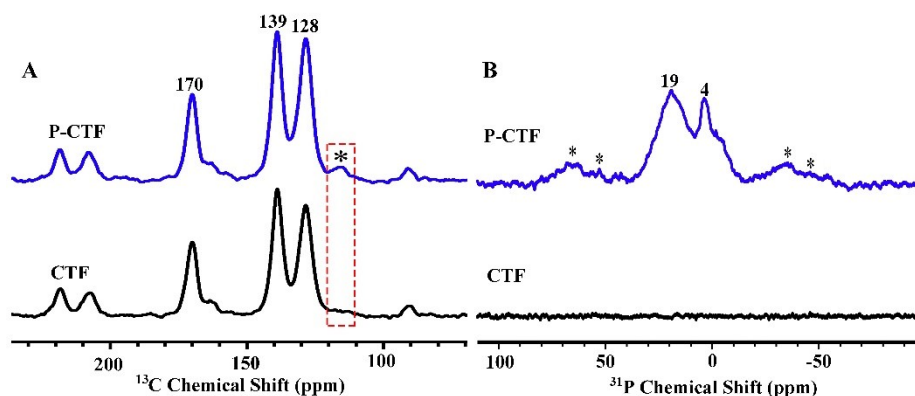


**Figure S10.** solid-state  $^{13}\text{C}$  (A) and  $^{31}\text{P}$  (B) NMR spectra of P-CTF and CTF samples.

### Additional discussions

As shown in Figure S10, the solid-state cross-polarization magic angle spinning carbon-13 and phosphorus-31 nuclear magnetic resonance ( $^{13}\text{C}$ -NMR and  $^{31}\text{P}$ -NMR) have been further performed to unveil the bonding sites and chemical state of phosphorus atoms in P-CTF. The  $^{13}\text{C}$ -NMR spectra of pristine CTFs clearly indicate that all the samples exhibited three obvious signals. Specifically, the chemical shifts at 128.0 and 139.0 ppm could be assigned to phenyl carbons, and the chemical shift at 170.0 ppm is indexed to the carbon signal from triazine rings<sup>15-17</sup>. For the P-CTF samples, a new peak at 115 ppm has been observed in the  $^{13}\text{C}$ -NMR spectrum. Combining with the XPS and FTIR results, this peak should be attributed to the bonding of the C2c with P atoms in the benzene ring structure. Moreover, the two new signals centered on 19 ppm and 4 ppm have also been detected in  $^{31}\text{P}$ -NMR spectra of P-CTF samples, which should be attributed to the P-C coordination in the framework and P-O bond, respectively<sup>18</sup>.

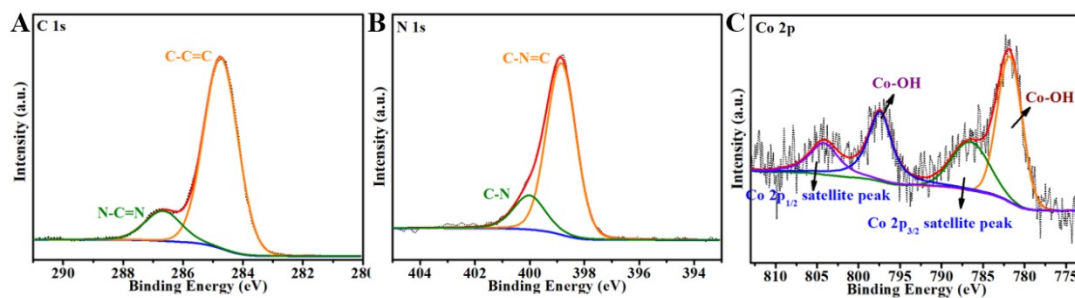


**Figure S11.** High-resolution (A) C 1s, (B) N 1s and (C) Co 2p XPS spectra of CTF-Co(OH)<sub>2</sub>.

**Additional discussion:**

From the XPS spectra, compared with P-CTF-Co<sub>2</sub>P, there is no P-C peak and Co-P peak in CTF-Co(OH)<sub>2</sub> sample, further indicating the successful formation of Co<sub>2</sub>P cocatalysts in the phosphidation process.

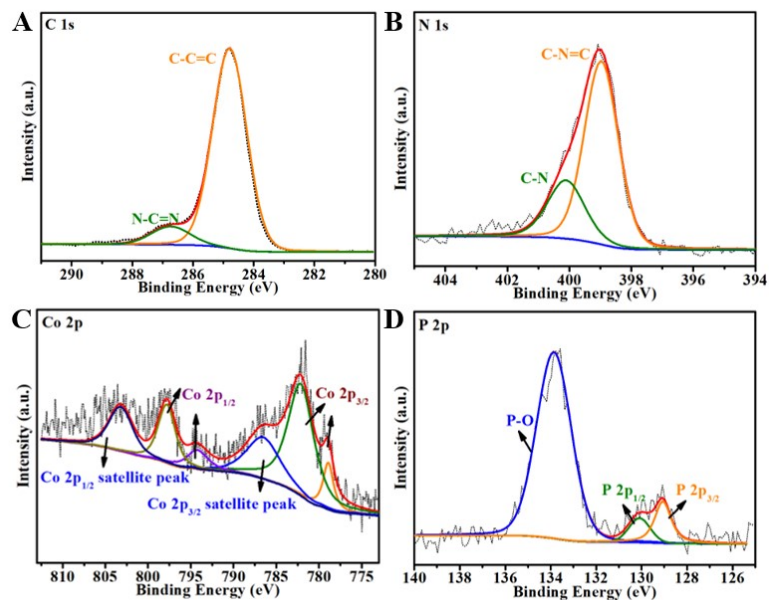


**Figure S12.** High-resolution (A) C 1s, (B) N 1s, (C) Co 2p and (D) P 2p XPS spectra of CTF/Co<sub>2</sub>P composite.

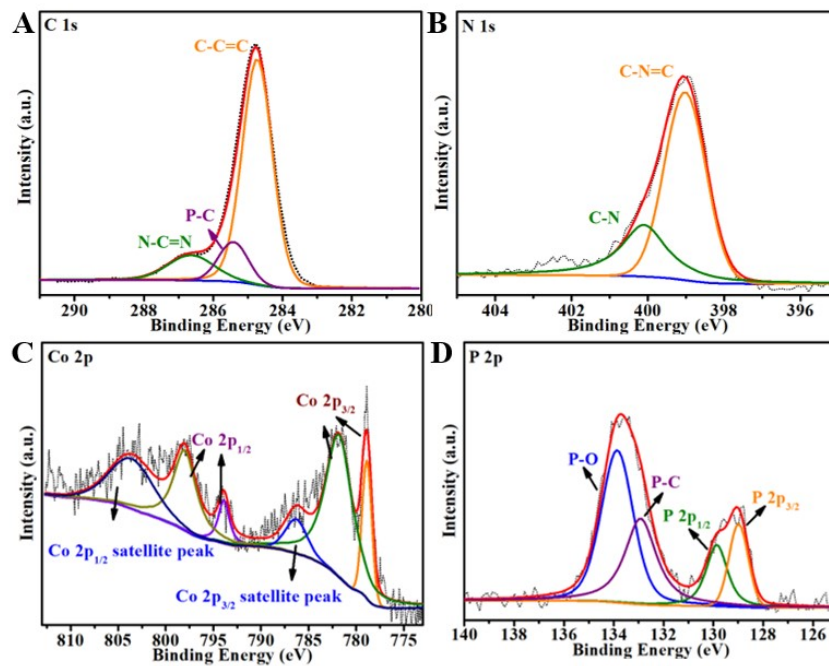


**Figure S13.** High-resolution (A) C 1s, (B) N 1s, (C) Co 2p and (D) P 2p XPS spectra of P-CTF/Co<sub>2</sub>P composite.

**Table S2.** The relative ratio of C-C=C to N-C=N bonds of CTF/Co<sub>2</sub>P and P-CTF/Co<sub>2</sub>P sample.

Photocatalyst	The peak area of C-C=C (S <sub>1</sub> )	The peak area of N-C=N (S <sub>2</sub> )	The relative ratio of S <sub>1</sub> /S <sub>2</sub>
CTF/Co <sub>2</sub> P	12004.0	1222.9	9.8
P-CTF/Co <sub>2</sub> P	9148.9	1564.3	5.8

#### Additional discussion:

Because of no phosphidation process in CTF/Co<sub>2</sub>P, the ratio of C-C=C to N-C=N is nearly similar to that of CTF. In P-CTF/Co<sub>2</sub>P, the ratio of C-C=C to N-C=N is nearly similar to that of P-CTF, further demonstrating the P-C bonding and their anchoring with Co<sub>2</sub>P cocatalysts in P-CTF-Co<sub>2</sub>P, different from CTF/Co<sub>2</sub>P and P-CTF/Co<sub>2</sub>P.

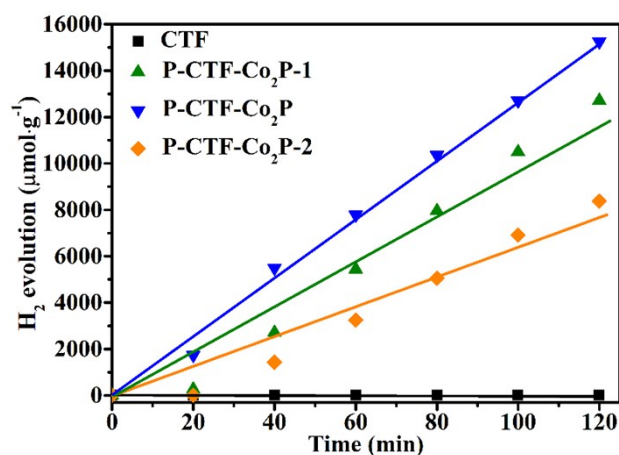


**Figure S14.** Photocatalytic H<sub>2</sub> generation of CTF and P-CTF-Co<sub>2</sub>P catalysts under light irradiation.

### Additional discussion

As shown in Figure S14, the effects of Co<sub>2</sub>P ratios on the photocatalytic performances have been studied. With reducing Co<sub>2</sub>P ratio down to 1 wt% (P-CTF-Co<sub>2</sub>P-1), the hydrogen evolution rate has been decreased from 15.2 to 12.7 mmol·g<sup>-1</sup> in 2 hours. In contrast, by increasing Co<sub>2</sub>P ratio up to 4 wt% (P-CTF-Co<sub>2</sub>P-2), the hydrogen evolution rate has been also decreased down to 8.4 mmol·g<sup>-1</sup>. Therefore, the rational incorporation of Co<sub>2</sub>P nanosheets and CTF with proper ratios should be crucial to achieve the optimal activity.

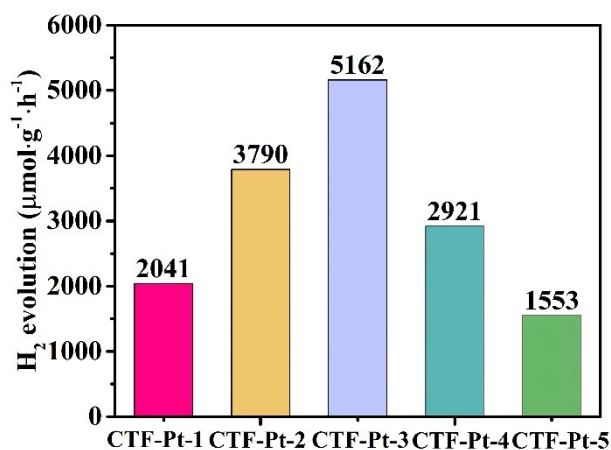


**Figure S15.** The hydrogen evolution rates of CTF-Pt catalysts under 2 h light irradiation.

### Additional discussion

To further investigate the relationship between metal Pt loadings and photocatalytic activities, the Pt loaded-catalysts (CTF-Pt) have been prepared and these hydrogen evolution rate have also

been listed in Figure S15. On the basis of above results, it can be concluded that the increase of metal Pt amounts on CTF within a proper range should also be effective for promoting the hydrogen production activity. However, with increasing the metal Pt loading amounts (CTF-Pt-4 and CTF-Pt-5), the hydrogen evolution activities have been evidently decreased. Therefore, the in-situ bonding of  $\text{Co}_2\text{P}$  cocatalysts on CTFs should be a promising strategy for achieving the highly efficient photocatalytic hydrogen evolution.

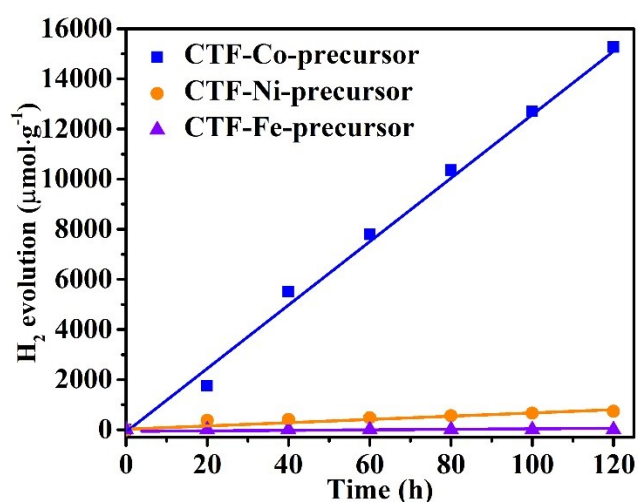


**Figure S16.** The hydrogen evolution of CTF-Co-precursor (P-CTF- $\text{Co}_2\text{P}$ ), CTF-Ni-precursor, CTF-Fe-precursor catalysts under 2 h light irradiation.

### Additional discussion

This one-step phosphidation strategy could serve as a universe strategy for anchoring other metal phosphides on CTFs. The Fe- and Ni-based phosphides have also been fabricated by the same process, and their hydrogen production activities have been studied under same conditions. As shown in Figure S16, compared with the P-CTF- $\text{Co}_2\text{P}$  samples, these Fe- and Ni-based phosphides anchored CTFs exhibited much lower  $\text{H}_2$  evolution activities. Furthermore, these demonstrations clearly indicate that the Co-based phosphides should be more efficient for promoting the hydrogen production activities of CTFs.

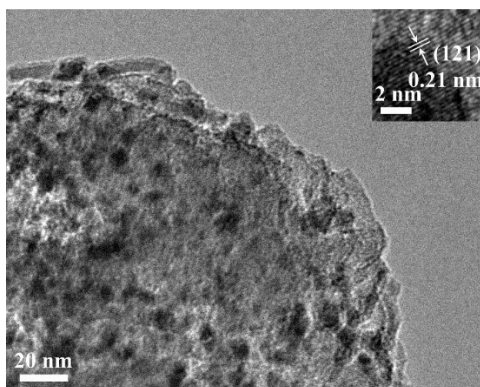


Figure S17. the TEM image of P-CTF-Co<sub>2</sub>P sample tested after photocatalytic reaction.

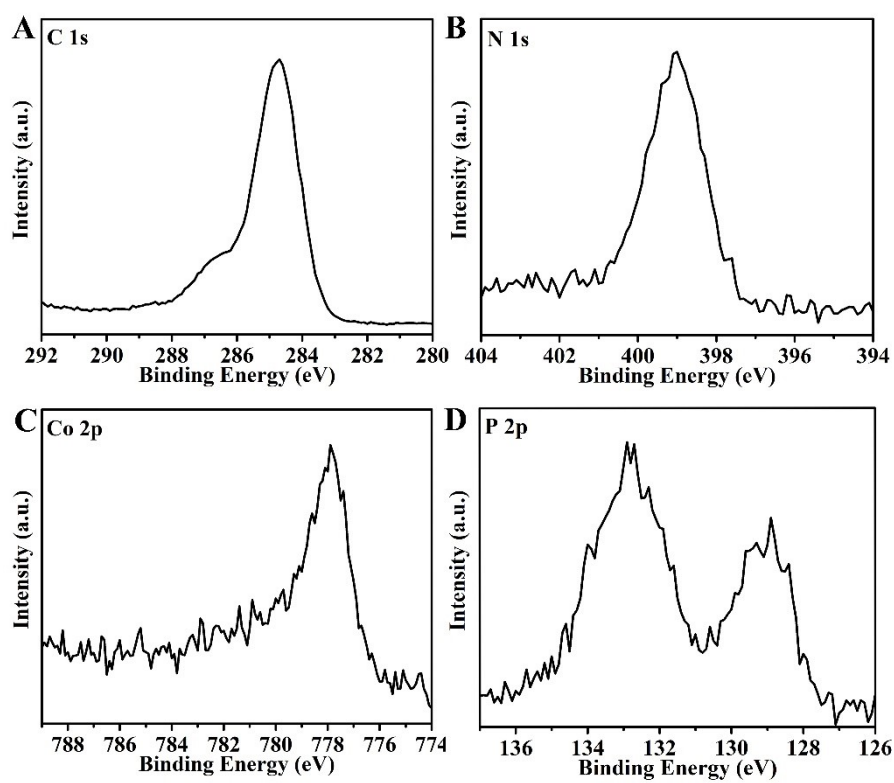
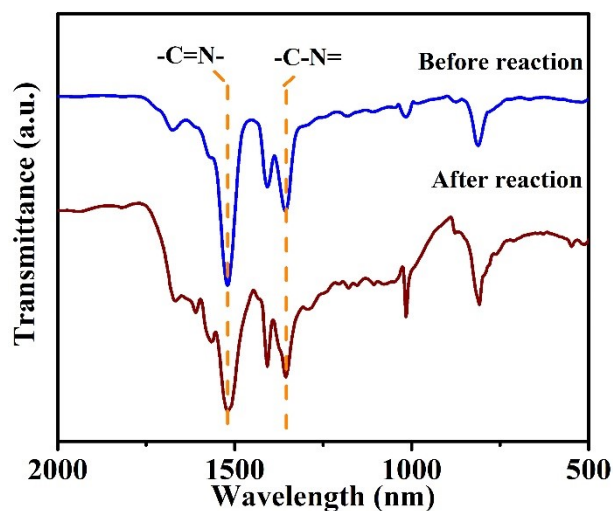


Figure S18. The XPS spectra of P-CTF-Co<sub>2</sub>P sample tested after photocatalytic reaction.



**Figure S19.** The FTIR spectrum before and after photocatalytic experiment of the P-CTF-Co<sub>2</sub>P sample.

### Additional discussion

To investigate the stability of P-CTF-Co<sub>2</sub>P, ten cycling H<sub>2</sub> photocatalytic production experiments has been conducted (Figure 3D). Clearly, it can be observed that H<sub>2</sub> was continuously generated without noticeable deviations. Moreover, after the cycling reaction, the structure and morphology of the P-CTF-Co<sub>2</sub>P sample have also been performed. From the results of TEM, XPS and FTIR (Figure S17-19), there is no structural and morphological changes occurred in the used P-CTF-Co<sub>2</sub>P sample after the photocatalytic reaction.

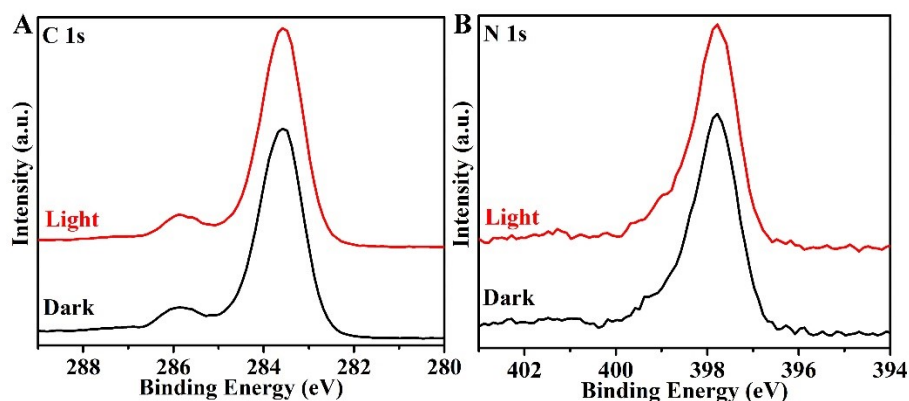


**Figure S20.** High-resolution (A) C 1s, (B) N 1s XPS spectra of pure CTF sample tested in darkness and under illumination.

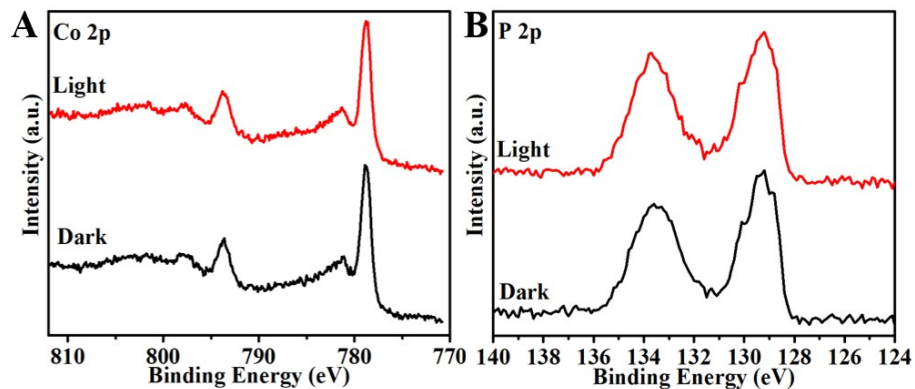


**Figure S21.** High-resolution (A) Co 2p and (B) P 2p XPS spectra of pure Co<sub>2</sub>P sample tested in darkness and under illumination.

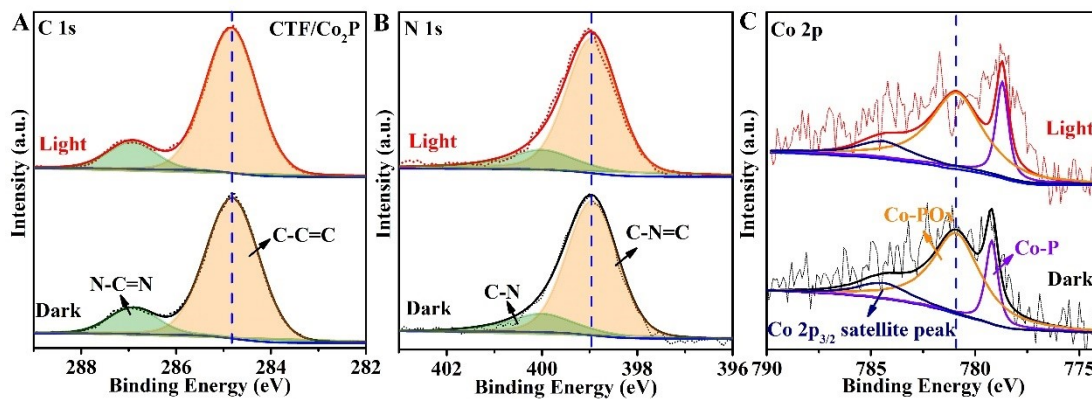


**Figure S22.** High-resolution (A) C 1s, (B) N 1s and (C) Co 2p XPS spectra of CTF/Co<sub>2</sub>P sample tested in darkness and under illumination.

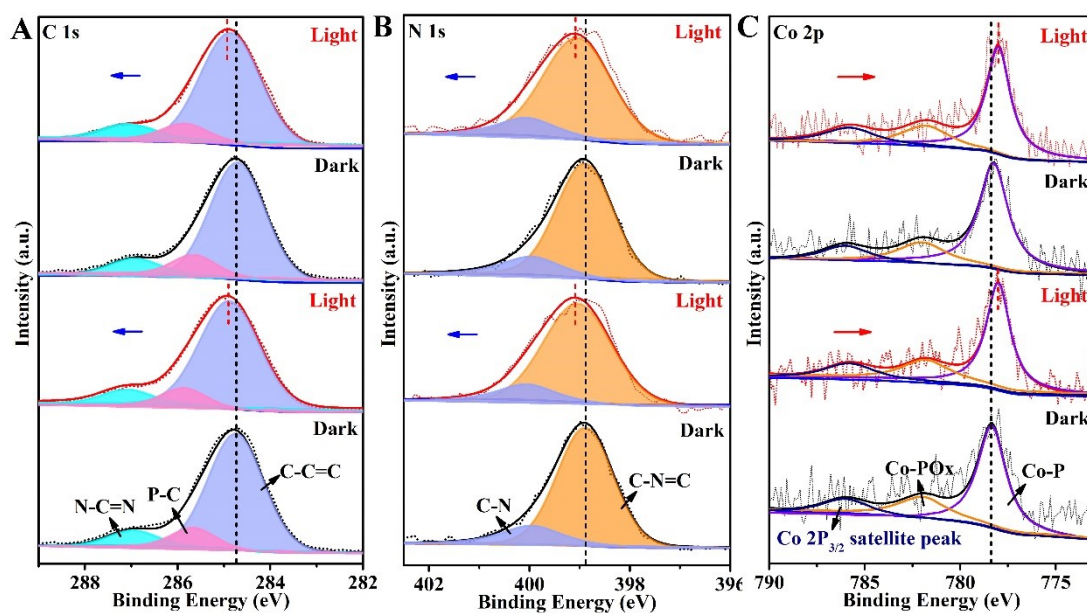


Figure S23. The cyclic SI-XPS of P-CTF-Co<sub>2</sub>P sample.

### Additional discussion

The SI-XPS tests under alternate light and dark have been performed for four times. As shown in Figure S23, the BE shifts and shape changes could also be observed again in the 2nd-light irradiation. Moreover, the samples return to the origin states in the 2nd dark. Thereby, these demonstrations clearly reveal that the charge transfer between CTF and Co<sub>2</sub>P of P-CTF-Co<sub>2</sub>P samples should be highly reversible, which could facilitate the stable H<sub>2</sub> evolution activity during the photocatalytic process.

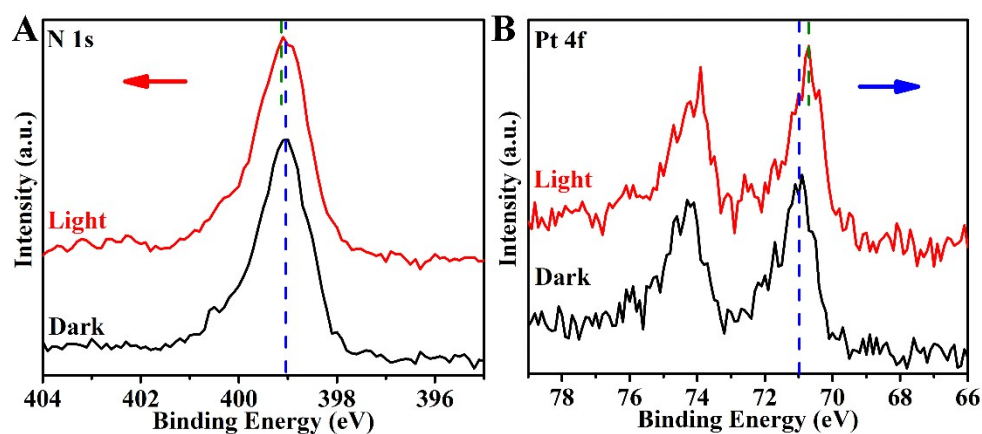


Figure S24. High-resolution (A) N 1s and (B) Pt 4f XPS spectra of CTF-Pt sample tested in darkness and under illumination.

### Additional discussion

As shown in Figure S24, there was a positive shift in the N 1s binding energy, suggesting a decrease in its electron density of CTF under light irradiation. And the Pt 4f peak shifted towards the low BE direction, indicating the electron enrichment in the Pt sites. It can be clearly seen that the photo-generated electron transfer from CTF to Pt under light irradiation.

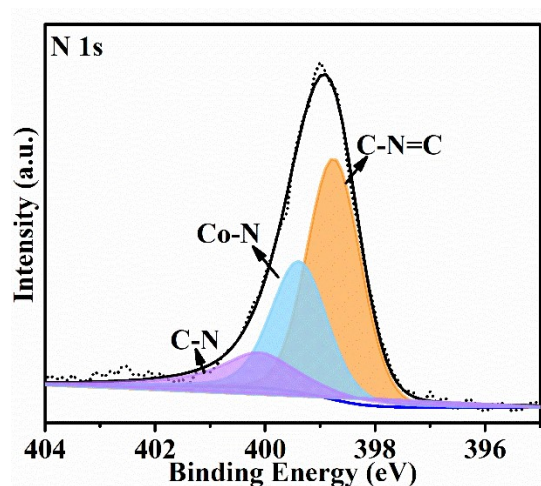
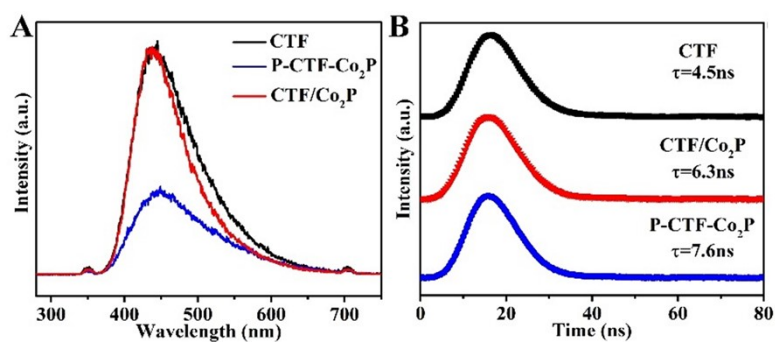


Figure S25. High-resolution N 1s XPS spectra of P-CTF-Co<sub>2</sub>P-Co sample.



**Figure S26.** (A) Photoluminescence spectra, (B) time-resolved photoluminescence spectra monitored at 500 nm of CTF, CTF/Co<sub>2</sub>P and P-CTF-Co<sub>2</sub>P. All samples are excited with 355 nm light from a pulsed laser (1 mg/ml).

### Additional discussions

The steady-state and time-resolved photoluminescence (PL) spectra were performed to further explore the photo-generated carrier recombination. As shown in Figure S26, the PL intensity of P-CTF-Co<sub>2</sub>P sample has been significantly decreased compared with pure CTF and CTF/Co<sub>2</sub>P, which demonstrates the high charge separation and transfer efficiency through the interfacial P-C bonding. Furthermore, time-resolved photoluminescence (TR-PL) spectroscopy was employed to analyze the behavior of charge separation and recombination kinetics. The TR-PL results reveal that the resulting fluorescent lifetime for P-CTF-Co<sub>2</sub>P is 7.6 ns, higher than that of CTF (4.5 ns) and CTF/Co<sub>2</sub>P (6.3 ns). The increased lifetime and the quenched PL intensity of P-CTF-Co<sub>2</sub>P should be attributed to suppressed charge recombination of the excited state.

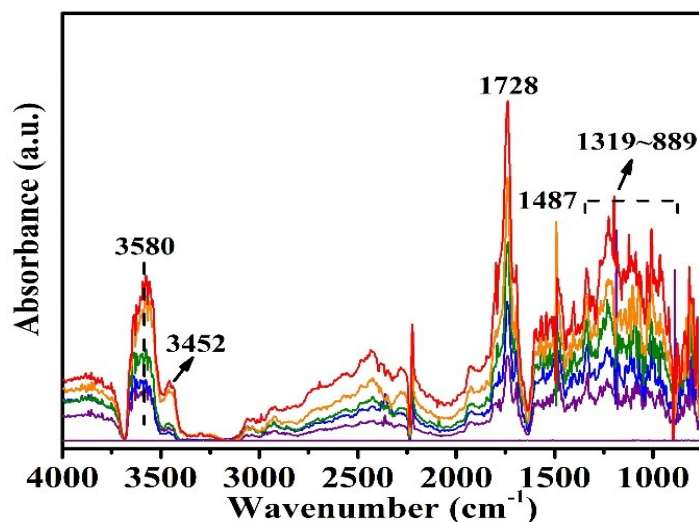


**Figure S27.** In situ FTIR spectra for co-adsorption of H<sub>2</sub>O vapor on the P-CTF-Co<sub>2</sub>P sample.

### Additional discussions

Moreover, the in-situ FTIR spectra have been conducted on P-CTF-Co<sub>2</sub>P sample in H<sub>2</sub>O atmosphere under light-irradiation. As shown in Fig. S27, with increasing light-irradiation time,

the increased water dissociation peaks in the range of  $3450 \sim 3580 \text{ cm}^{-1}$  could be evidently observed. Moreover, the broad absorption peaks from  $1319$  to  $889 \text{ cm}^{-1}$  attributed to the stretching vibration of C-O and breakage of O-H bonds could also be detected in the original ranges of triazine rings during the photocatalytic process.<sup>19-22</sup> These demonstrations clearly reveal that water oxidation reaction should be occurred in the triazine rings of CTFs structure, which was also consistent with the change transfer direction of in-situ XPS results.

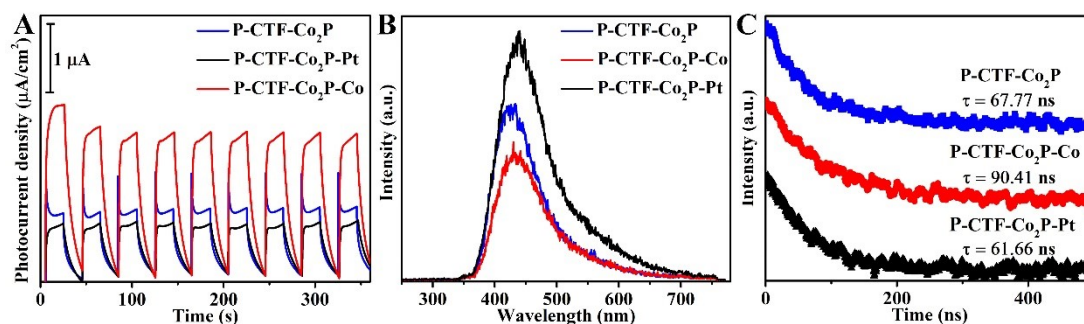


**Figure S28.** (A)  $I-t$  curves at  $-0.3 \text{ V}$  (vs. SCE); (B) Photoluminescence spectra; (C) time-resolved transient absorption spectroscopy (TAS) monitored at  $600 \text{ nm}$  of P-CTF- $\text{Co}_2\text{P}$ , P-CTF- $\text{Co}_2\text{P-Co}$  and P-CTF- $\text{Co}_2\text{P-Pt}$ . All samples are excited with  $355 \text{ nm}$  light from a pulsed laser ( $0.1 \text{ mg/ml}$ ).

### Additional discussions

Based on the reviewer's suggestion, the amperometric  $I-t$  curves, steady photoluminescent (PL) and transient absorption spectroscopy have been performed to further explore their charge separation capability. As shown in Figure S28A,  $I-t$  curves clearly reveal that P-CTF- $\text{Co}_2\text{P-Co}$  exhibited higher photocurrent density than pristine P-CTF- $\text{Co}_2\text{P}$  and P-CTF- $\text{Co}_2\text{P-Pt}$  samples, confirming its more efficient charge separation capability. Moreover, the PL spectra (Figure S28B) clearly reveal that compared with P-CTF- $\text{Co}_2\text{P}$ , the Co incorporation could effectively decrease peak intensity, indicating the enhanced charge separation efficiency in P-CTF- $\text{Co}_2\text{P-Co}$ . In contrast, the PL intensity has been significantly increased after the Pt incorporation. Additionally, Figure S28C shows the time-resolved transient absorption spectroscopy (TAS) to probe the relaxation course of charge carrier dynamics. It can be clearly observed that the lifetime of transient signal of P-CTF- $\text{Co}_2\text{P-Co}$  sample could achieve up to  $90.41 \text{ ns}$ , which is longer lifetime than that of P-CTF- $\text{Co}_2\text{P}$  ( $67.77 \text{ ns}$ ) and P-CTF- $\text{Co}_2\text{P-Pt}$  ( $61.66 \text{ ns}$ ). On the basis of above results,

it can be concluded that the Co incorporation could further promote the charge separation attributed to effective hole trapping, while Pt incorporation exhibited the negative effects owing to its competitions with Co<sub>2</sub>P for electron trapping. The related results and discussions have been added into the revised manuscript and supporting information.

**Table S3.** Summarized representative metal-free activated photocatalysts for H<sub>2</sub> production

Photocatalyst	The loadings of Pt element	H <sub>2</sub> evolution rate (μmol·h <sup>-1</sup> ·g <sup>-1</sup> )	Reference
CTF-HUST-2	3wt%	2647	2
CTF-1	3wt%	1072	23
CTF-N	1wt%	2060	24
CTF-BT/Th-1	3wt%	6600	25
CTF-15	3wt%	2946	26
CTF-HS <sub>0.75</sub> -1	3wt%	6040	27
CTF-2	3wt%	45	28
CTF-0-M2	3wt%	1030	29
<del>BPE-C</del> CTF-T1	1 wt%	250	30
FL-CTF-2	3wt%	1527	31
PCTF-8	2.3wt%	118	32
B-BT-1.4	3wt%	400	33
TFPT-COF	3wt%	1970	34
N <sub>3</sub> -COF	3wt%	1703	35
CTF-HUST-C1	3wt%	5100	36
<b>P-CTF-Co<sub>2</sub>P</b>	<b>-</b>	<b>7632</b>	<b>This work</b>

## References:

1. M. Liu, Q. Huang, S. Wang, Z. Li, B. Li, S. Jin, B. Tan, *Angew. Chem. Int. Ed.* 2018, 57 (37), 11968-11972.
2. K. Wang, L. Yang, X. Wang, L. Guo, G. Cheng, C. Zhang, S. Jin, B. Tan, A. Cooper, *Angew. Chem. Int. Ed.* 2017, 56, 14149-14153.
3. T. Wächter, K. J. Scheetz, A. D. Spaeth, M. V. Barybin, M. Zharnikov, *J. Phys. Chem. C*, 2017, 121, 13777;
4. Y. Pan, S. Liu, K. Sun, X. Chen, B. Wang, K. Wu, X. Cao, W. Cheong, R. Shen, A. Han, Z. Chen, L. Zheng, J. Luo, Y. Lin, Y. Liu, D. Wang, Q. Peng, Q. Zhang, *Angew. Chem. Int. Ed.*, 2018, 57, 8614.
5. C. Lu, J. Yang, S. Wei, S. Bi, Y. Xia, M. Chen, Y. Hou, M. Qiu, C. Yuan, Y. Su, F. Zhang, H. Liang, X. Zhuang, *Adv. Funct. Mater.*, 2019, 29, 1806884.
6. P. Chen, T. Zhou, L. Xing, K. Xu, Y. Tong, H. Xie, L. Zhang, W. Yan, W. Chu, C. Wu, Y. Xie, *Angew. Chem.* 2017, 129, 625-629.
7. J. H. Lee, J. Ryu, J. Y. Kim, S. Nam, J. H. Han, T. Lim, S. Gautam, K. H. Chae, C. W. Yoon, *J. Mater. Chem. A*, 2014, 2, 9490-9495.
8. Z. Cheng, K. Zheng, G. Lin, S. Fang, L. Li, J. Bi, J. Shen, L. Wu, *Nanoscale Adv.*, 2019, 1, 2674.
9. L. Li, W. Fang, P. Zhang, J. Bi, Y. He, J. Wang, W. Su, *J. Mater. Chem. A*, 2016, 4, 12402;
10. S. Wang, F. He, X. Zhao, J. Zhang, Z. Ao, H. Wu, Y. Yin, L. Shi, X. Xu, C. Zhao, S. Wang, H. Sun, *Appl. Catal. B-Environ.*, 2019, 257, 117931.
11. M. Liu, Q. Huang, S. Wang, Z. Li, B. Li, S. Jin, B. Tan, *Angew. Chem. Int. Ed.*, 2018, 57, 11968-11972;
12. Y. Zhao, KX Yao, B. Teng, T. Zhang, Y. Han, *Energy Environ. Sci.*, 2013, 6, 3684-3692;
13. K. Wang, L. Yang, X. Wang, L. Guo, G. Cheng, C. Zhang, S. Jin, B. Tan, A. Cooper, *Angew. Chem. Int. Ed.*, 2017, 56, 14149-14153
14. X. Zhou, J. Jin, X. Zhu, J. Huang, J. Yu, W.-Y. Wong, W.-K. Wong, *J. Mater. Chem. A*, 2016, 4, 5282.
15. Z. Cheng, K. Zheng, G. Lin, S. Fang, L. Li, J. Bi, J. Shen, L. Wu, *Nanoscale Adv.*, 2019, 1, 2674.
16. L. Li, W. Fang, P. Zhang, J. Bi, Y. He, J. Wang, W. Su, *J. Mater. Chem. A*, 2016, 4, 12402.
17. S. Wang, F. He, X. Zhao, J. Zhang, Z. Ao, H. Wu, Y. Yin, L. Shi, X. Xu, C. Zhao, S. Wang, H. Sun, *Appl. Catal. B-Environ.*, 2019, 257, 117931.
18. P. Qiu, C. Xu, N. Zhou, H. Chen, F. Jiang, *Appl. Catal. B-Environ.*, 2018, 221, 27-35.
19. H. Sheng, H. Zhang, W. Song, H. Ji, W. Ma, C. Chen, J. Zhao, *Angew. Chem. Int. Ed.* 2015, 54, 5905-5909;
20. L. Ye, Z. Ma, Y. Deng, Y. Ye, L. Wang, M. Kou, H. Xie, Z. Xu, Y. Zhou, D. Xia, P. K. Wong, *Appl. Catal. B* 2019, 257, 117897;
21. C. A. Roberts, S. P. Phivilay, I. E. Wachs, *Chin. Chem. Lett.* 2018, 29, 769-772;
22. Z. Yu, S. S. C. Chuang, *J. Catal.* 2007, 246, 118-126
23. S. Kuecken, A. Acharjya, L. Zhi, M. Schwarze, R. Schomacker, A. Thomas, *Chem Commun.*, 2017, 53, 5854-5857.
24. M. Liu, X. Wang, J. Liu, K. Wang, S. Jin, B. Tan, *ACS Appl. Mater. Interfaces*, 2020, 12, 12774-12782.
25. W. Huang, Q. He, Y. Hu, Y. Li, *Angew. Chem. Int. Ed.*, 2019, 58, 8676-8680.
26. C. B. Meier, R. Clowes, E. Berardo, K. E. Jelfs, M. A. Zwijnenburg, R. S. Sprick, A. I. Cooper, *Chem. Mater.*, 2019, 31, 8830-8838.
27. S. Wang, B. Zhu, M. Liu, L. Zhang, J. Yu, M. Zhou, *Appl. Catal. B: Environ.*, 2019, 243, 19-26.
28. C. B. Meier, R. S. Sprick, A. Monti, P. Guiglion, J.-S. M. Lee, M. A. Zwijnenburg, A. I. Cooper, *Polymer*, 2017, 126, 283-290.
29. D. Kong, X. Han, J. Xie, Q. Ruan, C. D. Windle, S. Gadipelli, K. Shen, Z. Bai, Z. Guo, J. Tang, *ACS Catal.*, 2019, 9, 7697-7707.
30. J. Bi, W. Fang, L. Li, J. Wang, S. Liang, Y. He, M. Liu, L. Wu, *Macromol. Rapid Commun.*, 2015, 36, 1799-

805.

31. L. Li, Y. Zhu, N. Gong, W. Zhang, W. Peng, Y. Li, F. Zhang, X. Fan, *Int. J. Hydrog. Energy*, 2020, 45, 2689-2698.
32. A. Bhunia, D. Esquivel, S. Dey, R. Fernández-Terán, Y. Goto, S. Inagaki, P. Van Der Voort, C. Janiak, *J. Mater. Chem. A*, 2016, 4, 13450-13457.
33. C. Yang, B. C. Ma, L. Zhang, S. Lin, S. Ghasimi, K. Landfester, K. A. Zhang, X. Wang, *Angew. Chem. Int. Ed.*, 2016, 55, 9202-9206.
34. L. Stegbauer, K. Schwinghammer, B. V. Lotsch, *Chem. Sci.*, 2014, 5, 2789-2793.
35. V. S. Vyas, F. Haase, L. Stegbauer, G. Savasci, F. Podjaski, C. Ochsenfeld, B. V. Lotsch, *Nat. Commun.*, 2015, 6, 8508.
36. M. Liu, Q. Huang, S. Wang, Z. Li, B. Li, S. Jin, B. Tan, *Angew. Chem. Int. Ed.*, 2018, 57, 11968-11972.